

SPITZER SPACE TELESCOPE SPECTROSCOPY OF ICES TOWARD LOW MASS EMBEDDED PROTOSTARS[†]

A. C. ADWIN BOOGERT¹, KLAUS M. PONTOPPIDAN², FRED LAHUIS^{2,3}, JES K. JØRGENSEN², JEAN-CHARLES AUGEREAU², GEOFFREY A. BLAKE⁴, TIMOTHY Y. BROOKE¹, JOANNA BROWN¹, C. P. DULLEMOND⁵, NEAL J. EVANS, II⁶, VINCENT GEERS², MICHIEL R. HOGERHEIJDE², JACQUELINE KESSLER-SILACCI⁶, CLAUDIA KNEZ⁶, PAT MORRIS⁷, ALBERTO NORIEGA-CRESPO⁷, FREDRIK L. SCHÖIER², EWINE F. VAN DISHOECK², LORI E. ALLEN⁸, PAUL M. HARVEY⁶, DAVID W. KOERNER⁹, LEE G. MUNDY¹⁰, PHILIP C. MYERS⁸, DEBORAH L. PADGETT⁷, ANNEILA I. SARGENT¹, KARL R. STAPELFELDT¹¹

Submitted 26 March 2004; accepted 14 May 2004; scheduled for publication in ApJS Sept. 2004, v154 [Spitzer Special issue]

ABSTRACT

Sensitive 5–38 μm Spitzer Space Telescope (SST) and ground based 3–5 μm spectra of the embedded low mass protostars B5 IRS1 and HH46 IRS show deep ice absorption bands superposed on steeply rising mid-infrared continua. The ices likely originate in the circumstellar envelopes. The CO₂ bending mode at 15 μm is a particularly powerful tracer of the ice composition and processing history. Toward these protostars, this band shows little evidence for thermal processing at temperatures above 50 K. Signatures of lower temperature processing are present in the CO and OCN[−] bands, however. The observed CO₂ profile indicates an intimate mixture with H₂O, but not necessarily with CH₃OH, in contrast to some high mass protostars. This is consistent with the low CH₃OH abundance derived from the ground based L band spectra. The CO₂/H₂O column density ratios are high in both B5 IRS1 and HH46 IRS ($\sim 35\%$). Clearly, the SST spectra are essential to study ice evolution in low mass protostellar environments, and to eventually determine the relation between interstellar and solar system ices.

Subject headings: Infrared: ISM—ISM: molecules—ISM: abundances—stars: formation—stars: individual (B5 IRS1)—astrochemistry

1. INTRODUCTION

A recurring question in disk, planet and comet formation studies is how the composition of molecular material evolves as it flows from the molecular cloud to the protostellar envelope and protoplanetary disk. Much of the material in these environments is frozen on grains. A plethora of processes, including heating by stellar photons, shocks related to accretion or outflow, cosmic ray

hits, and ultraviolet irradiation can change the ice structure and composition. The spectroscopic effects of these processes can be observed in the vibrational bands of the ices through infrared spectroscopy. Ices around high mass protostars have been extensively studied this way. Infrared Space Observatory (ISO) spectra have shown that in particular the ice structure is affected by heating from the central star. The simplicity of the ice composition does indicate that the formation of new species through ultraviolet irradiation or cosmic ray hits occurs at a low level at best. Observations of ices around low mass protostars have been limited due to the unavailability of much of the 5–20 μm spectral region, where many of the molecular bending mode transitions occur. In particular the CO₂ bending mode at 15 μm is a valuable tracer of ice structure and composition (Ehrenfreund et al. 1998; Gerakines et al. 1999). With the sensitive Infrared Spectrometer (IRS; Houck et al. 2004) on board of the Spitzer Space Telescope (SST; Werner et al. 2004) this band can now be observed for the first time at high quality in low mass systems.

Observation of two protostars are presented in this paper. B5 IRS1 (IRAS 03445+3242; Beichman et al. 1984; $L = 10 L_{\odot}$) is well studied at infrared and millimeter wavelengths (e.g. Charnley et al. 1990; Langer et al. 1996). The millimeter continuum emission is resolved on a few arcsec scale, and may originate in an inclined disk. The outflow has received most of the attention, and has a large opening angle leading to significant outflow/infall interaction. HH46 IRS (IRAS 08242-5050; $L = 12 L_{\odot}$) is also deeply embedded, and is also the driving source of a powerful outflow. SST imaging and spectroscopic observations of this source, focused on the outflow, are

*SOME OF THE DATA PRESENTED HEREIN WERE OBTAINED AT THE W.M. KECK OBSERVATORY, WHICH IS OPERATED AS A SCIENTIFIC PARTNERSHIP AMONG THE CALIFORNIA INSTITUTE OF TECHNOLOGY, THE UNIVERSITY OF CALIFORNIA AND THE NATIONAL AERONAUTICS AND SPACE ADMINISTRATION. THE OBSERVATORY WAS MADE POSSIBLE BY THE GENEROUS FINANCIAL SUPPORT OF THE W.M. KECK FOUNDATION.

[†]THE VLT/ISAAC SPECTRA WERE OBTAINED AT THE EUROPEAN SOUTHERN OBSERVATORY, PARANAL, CHILE, WITHIN THE OBSERVING PROGRAM 272.C-5008

¹ Division of PMA, Mail Code 105-24, California Institute of Technology, Pasadena, CA 91125, USA

² Leiden Observatory, PO Box 9513, 2300 RA Leiden, the Netherlands

³ SRON, PO Box 800, 9700 AV Groningen, the Netherlands

⁴ Division of GPS, Mail Code 150-21, California Institute of Technology, Pasadena, CA 91125, USA

⁵ Max-Planck-Institut für Astrophysik, P.O. Box 1317, D-85741 Garching, Germany

⁶ Department of Astronomy, University of Texas at Austin, 1 University Station C1400, Austin, TX 78712-0259

⁷ Spitzer Science Center, California Institute of Technology, CA 91125, USA

⁸ Smithsonian Astrophysical Observatory, 60 Garden Street, MS42, Cambridge, MA 02138

⁹ Department of Physics and Astronomy, Northern Arizona University, Box 6010, Flagstaff, AZ 86011-6010

¹⁰ Department of Astronomy, University of Maryland, College Park, MD 20742

¹¹ Jet Propulsion Laboratory, MS 183-900, California Institute of Technology, 4800 Oak Grove Drive, Pasadena, CA 91109

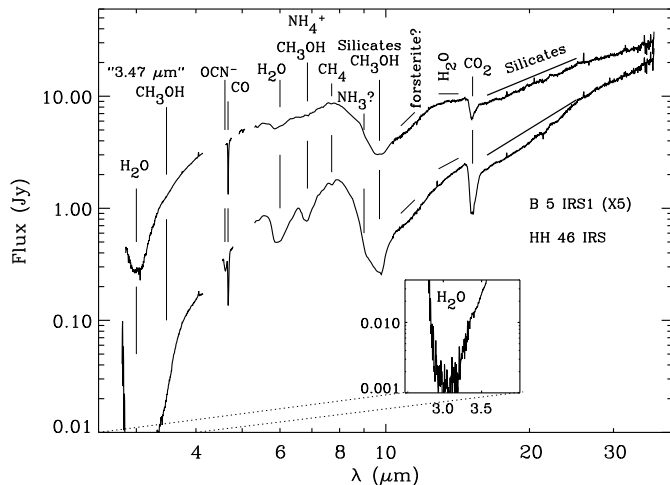


FIG. 1.— Combined Spitzer Space Telescope and ground based L and M band spectroscopy of B5 IRS1 (top, multiplied by factor of 5 for clarity) and HH46 IRS (bottom). Identifications and possible identifications are indicated.

presented in Noriega-Crespo et al. (2004).

2. OBSERVATIONS

B5 IRS1 and HH46 IRS were observed with SST/IRS as part of the ‘c2d’ Spitzer Legacy program (Evans et al. 2003) in the modules Short Low (SL; $\lambda = 5 - 14 \mu\text{m}$; $R=64-128$), Short High (SH; $\lambda = 10 - 20 \mu\text{m}$; $R=600$) and Long High (LH; $\lambda = 20 - 38 \mu\text{m}$; $R=600$). The archival AOR keys are 0005638912 (HH46 IRS) and 0005635328 (B5 IRS1) for PROGID 172. Both sources are well centered in all slits. The integration time was 28 seconds per module per source at 14 second ramps, except for SH which has 24 seconds in total and 6 second ramps. The spectra were reduced with the IRS pipeline version 9.5 on 10 March 2004 at the SSC. Bad pixels were interpolated in the spectral domain in the 2D images before extracting 1D spectra. Accurate wavelength calibration was assured using calibration tables available in May 2004. For overlapping SH spectral orders, the poorly calibrated long wavelength part of each order was removed. This is particularly important to obtain a reliable profile of the CO_2 ice band at $15.2 \mu\text{m}$, where two orders overlap. HH46 IRS was observed independently as an Early Release Observation (AOR key 0007130112 and PROGID 1063; Noriega-Crespo et al. 2004). The datasets are in good agreement, and were averaged. Finally, complementary ground based observations were obtained. B5 IRS1 was observed with Keck/NIRSPEC (McLean et al. 1998) at $R=25000$ in the M band and at $R=2000$ in the L band. VLT/ISAAC (Moorwood et al. 1999) L and M band spectra of HH46 IRS were obtained at $R=600$ and 5000 respectively. The SST and ground based spectra were combined by scaling the ground based data.

3. RESULTS

The combined SST and ground based $3-38 \mu\text{m}$ spectra of B5 IRS1 and HH46 IRS show steeply rising continua (Fig. 1). The continuum of HH46 IRS is the steep-

est, with a $35 \mu\text{m}/4 \mu\text{m}$ flux ratio of 100, compared to 10 for B5 IRS1. Numerous silicate and ice absorption features are superposed. The main ice constituents are H_2O , CO_2 , and CO . The well known, yet unidentified, 3.47 and $6.85 \mu\text{m}$ bands are present in both sources as well. Rarely seen before is a shallow absorption feature at $11.2 \mu\text{m}$ in both sources. It may be related to refractory dust components, such as crystalline forsterite (Kessler et al. 2004). In addition, HH46 IRS, but not B5 IRS1, shows absorption by CH_4 and ‘ XCN ’ (likely OCN^- ; van Broekhuizen et al. 2004). Finally, other ice features may be present in the $5-10 \mu\text{m}$ region (NH_3 , HCOOH), but a dedicated analysis is required to verify their reality. We focus on the band profiles and abundances of the main ice components and their relation to the $15 \mu\text{m}$ CO_2 bands, newly discovered with the SST.

The CO_2 bending mode has rarely been observed toward low mass protostars, and never at such high quality. It is blended with the short wavelength wing of the silicate bending mode. The CO_2 band is put on an optical depth scale, assuming the ‘intrinsic’ profile of the silicate band is represented by the Galactic Center source GC3 (Chiar et al. 2000). For this a third order polynomial is fitted to the wavelength regions $13.0-14.7$ and $26.3-33.3 \mu\text{m}$. The resulting CO_2 bands look similar to those observed in other lines of sight; note in particular the presence of a long wavelength wing extending to at least $16 \mu\text{m}$ (Gerakines et al. 1999). Similar to the massive protostar NGC 7538 IRS9 (Fig. 2b), weak double ice crystallization peaks are observed at the bottom of the band in HH46 IRS, but not in B5 IRS1. Neither B5 IRS1 nor HH46 IRS show evidence for a third peak at $15.38 \mu\text{m}$, expected in $\text{CH}_3\text{OH}:\text{CO}_2$ complex formation.

To place the interpretation of the CO_2 band within a larger perspective, ground based observations of the $3.53 \mu\text{m}$ CH_3OH band and the $4.67 \mu\text{m}$ band of solid CO are analyzed. The $3.53 \mu\text{m}$ band is superposed on the wing of the strong $3.07 \mu\text{m}$ H_2O band and is locally blended with the unidentified $3.47 \mu\text{m}$ band. Following Brooke et al. (1999), we derive the continuum and separate the CH_3OH contribution. For comparison, spectra of the massive protostars W33A (Brooke et al. 1999) and NGC 7538 IRS9 (Boogert et al. 2004) are analyzed as well. Hints of CH_3OH are seen in both HH46 IRS and B5 IRS1, resulting in column densities of 7% with respect to H_2O , comparable to NGC 7538 IRS9, but much less compared to W33A. For HH46 IRS the detection of CH_3OH is strengthened by the presence of a feature at $9.7 \mu\text{m}$ in the bottom of the silicate band (Fig. 1). Both HH46 IRS and B5 IRS1 show prominent bands of solid CO at $4.67 \mu\text{m}$ (Fig. 2d). The ratio between the central narrow CO component and the broad long wavelength wing, representing the column density ratio of volatile pure CO and CO mixed with less volatile H_2O , is a factor of five smaller in HH46 IRS. In fact, the profile of HH46 IRS is comparable to that of the massive protostar W33A. The latter two sources also show a band at $4.62 \mu\text{m}$, most likely attributed to the OCN^- ion. Relative to H_2O , the OCN^- column density is comparable to (upper limits to) those of B5 IRS1 and NGC7538 IRS9. Furthermore, the $4.67 \mu\text{m}$ spectrum of B5 IRS1 shows deep ro-vibrational gas phase CO lines. The presence of gas phase CO in HH46 IRS is hard to assess because of telluric contamination. The intriguing differences and similarities between

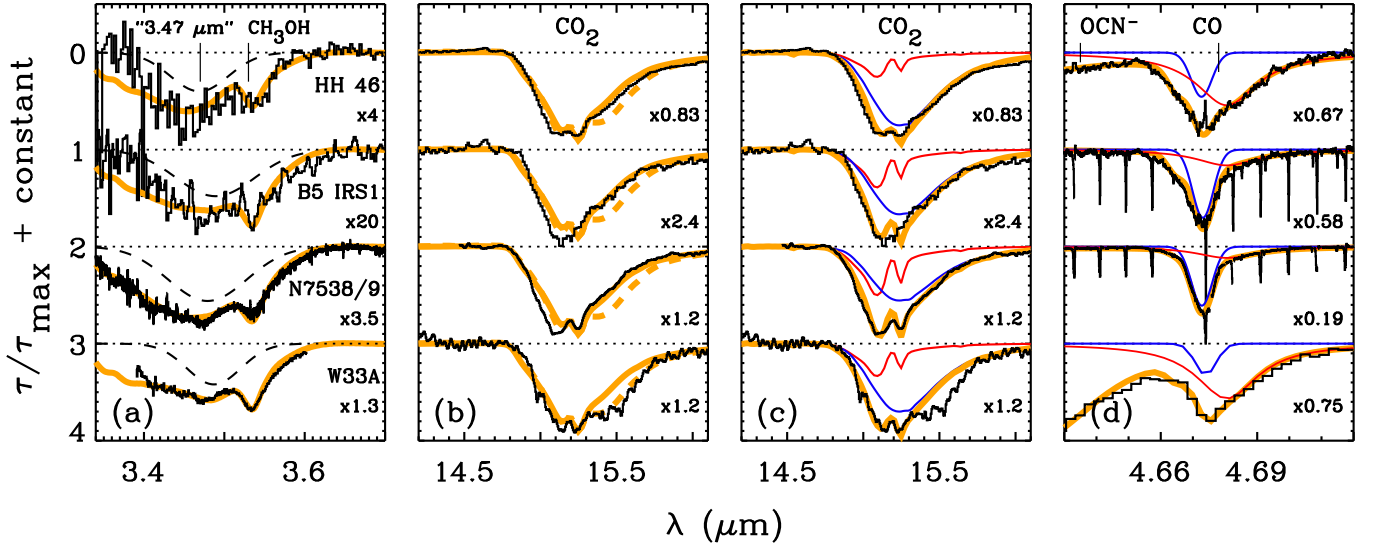


FIG. 2.— Solid CH₃OH (a), CO₂ (b and c), and CO (d) spectra of HH46 IRS and B5 IRS1 compared to the massive protostars NGC7538 IRS9 and W33A in each panel from top to bottom. The normalization factor is indicated in the right corner of each plot. **Panel a:** a laboratory pure CH₃OH spectrum at $T_{\text{lab}} = 10$ K (thick yellow line) to which is added a Gaussian (dashes) to account for the underlying “3.47 μm ” absorption feature. The NGC7538 IRS9 and W33A data are from Boogert et al. (2004) and Brooke et al. (1999) respectively. **Panel b:** the CO₂ bending mode observed with SST/IRS (HH46 IRS and B5 IRS1) and ISO/SWS (NGC 7538 IRS9 and W33A). The thick yellow dashed line is the laboratory ice H₂O:CH₃OH:CO₂=0.84:0.92:1, and the continuous thick yellow line is a laboratory ice with reduced CH₃OH content, H₂O:CH₃OH:CO₂=0.92:0.29:1, both at $T_{\text{lab}}=115$ K. Only for W 33A an enhanced CH₃OH/CO₂ ratio is required, in agreement with the strong 3.53 μm CH₃OH feature in panel (a). **Panel c:** the CO₂ bending mode for the same sources as in panel (b), but now fitted with different laboratory spectra: a highly processed polar ice ($T_{\text{lab}}=125$ K; red) in combination with an H₂O-rich, CH₃OH-deficient cold ice ($T_{\text{lab}}=10$ K; blue). The sum of these two components is the thick yellow line. **Panel d:** the absorption band of solid CO observed with VLT/ISAAC (HH46 IRS), Keck/NIRSPEC (B5 IRS1 and NGC7538 IRS9) and ISO/SWS (W33A). Narrow absorption lines are due to circumstellar gas phase CO. The onset of the 4.62 μm ‘XCN’ band is seen in HH46 IRS and W33A. Gaussian and Lorentzian fits to the apolar and polar CO components are indicated by blue and red lines respectively. The thick yellow line represents the combined fit, including the ‘XCN’ bands and blue-shifted CO component that are not shown separately.

HH46 IRS and B5 IRS1, as well as compared to massive protostars, provide insight into the formation and evolution of interstellar and circum-protostellar ices.

Finally, column densities of the main ices, summarized in Table 1, are derived by dividing the integrated optical depth over the laboratory integrated band strength (e.g. Hudgins et al. 1993). Note that the CO₂/H₂O ratios toward B5 IRS1 and HH46 IRS are significantly larger compared to the average over many, mostly massive protostellar sightlines (0.17 ± 0.03 ; Gerakines et al. 1999).

4. DISCUSSION

4.1. Evolution of Ices in Low Mass Environments

The formation and evolution of interstellar ices is, in principle, strongly dependent on local conditions such as the atomic hydrogen and carbon density, the temperature, the cosmic ray flux, the ultraviolet photon flux, and the presence of shocks. Thus, key issues are the location of the ices along the absorption line of sight and the relative contributions from foreground clouds, envelopes, and inclined disks. The continuous rise of both the B5 IRS1 and HH46 IRS SEDs between 3 and 40 μm , as well as the detection of extended submillimeter emission in JCMT archive images, are in favor of envelope-dominated models. We established the properties of these envelopes using the approach of Jørgensen et al. (2002). Adopting optical constants for bare and ice coated silicate grains

(Ossenkopf & Henning 1994) the 2-2000 μm SED and the depth of the observed superposed ice and silicate bands were self-consistently modeled. The SED and silicate band depth of B5 IRS1 are well fitted by the envelope models, and a significant fraction of the ices has evaporated. In contrast to B5 IRS1, the submillimeter/far-infrared and mid-infrared SST SED of HH46 IRS cannot be simultaneously fitted. Possibly, this envelope is embedded in a larger scale, cold cloud not modeled within the framework of the simple spherical envelope.

Next we address the extent to which the ices in these envelopes have been processed. Several indicators are available. Laboratory experiments have shown that heating of ice mixtures with concentrations CO₂/H₂O ≥ 1 results in crystallization and an effective segregation of the CO₂ and H₂O species. Spectroscopically this is recognized as double peaked profiles, characteristic of the pure CO₂ matrix (Ehrenfreund et al. 1998). Depending on the ice composition, the amorphous to crystalline phase transition occurs at 50-90 K in space, lower than the corresponding laboratory temperatures due to the longer interstellar time scales (Boogert et al. 2000). Substructures are seen in the HH46 IRS CO₂ band (Fig. 2b), but are much weaker compared to some highly heated massive protostellar envelopes (Gerakines et al. 1999), and are absent in B5 IRS1. In fact, the CO₂ band profile of HH46 IRS is comparable to that observed toward one of the least processed envelopes, surrounding the massive protostar NGC 7538 IRS9. In the simplest scenario of a single ice at one temperature, the mixture

TABLE 1
COLUMN DENSITIES AND ABUNDANCES

Quantity	B5 IRS1	HH46	N7538/9 ^e	W33A ^f
$N(\text{CO}_2)/N(\text{H}_2\text{O})$	0.37	0.32	0.24	0.16
$N(\text{CO-p})/N(\text{H}_2\text{O})^a$	0.16	0.15	0.02	0.08
$N(\text{CO-np})/N(\text{H}_2\text{O})^b$	0.27	0.05	0.14	0.03
$N(\text{CH}_3\text{OH})/N(\text{H}_2\text{O})$	<0.06	0.07	0.07	0.22
$N(\text{OCN}^-)/N(\text{H}_2\text{O})^c$	<0.005	0.007	0.006	0.02
$N(\text{H}_2\text{O}) [10^{18} \text{ cm}^{-2}]$	2.2 (0.3)	8.0	6.8	9.0
$N(\text{H}_2\text{O})/N_{\text{H}} [10^{-5}]$	5.2	5.7	5.0	3.2
$N_{\text{H}} [10^{22} \text{ cm}^{-2}]$	4 ^d	14 ^d	16	28

^a broad ‘polar’ CO component, likely H_2O mixture

^b broad ‘apolar’ CO component, likely pure CO

^c using OCN^- band strength of van Broekhuizen et al. 2004

^d from the envelope models described in the text

^e Whittet et al. 1996 and references therein

^f Gibb et al. 2000 and references therein

$\text{CH}_3\text{OH}:\text{H}_2\text{O}:\text{CO}_2=0.3:1:1$ (§4.2) must still have a laboratory temperature as high as 115 K, or ~ 75 K in space (Fig. 2b). In the more likely scenario of a temperature gradient along the line of sight, the bulk of the HH46 IRS and B5 IRS1 envelopes have temperatures well below 50 K. A fraction of the inner envelope of HH46 IRS must be warmer, causing the observed weak substructures. Such two component fits explain the observed profiles well (Fig. 2c).

More extensive processing at lower temperatures most likely has occurred within the envelopes, however. Unlike the massive protostar NGC 7538 IRS9, the ground based $4.67 \mu\text{m}$ spectra of solid CO toward HH46 IRS and B5 IRS1 show a weak central narrow component (Fig. 2d; Table 1). The most volatile CO-rich ‘apolar’ ices may thus have evaporated (Tielens et al. 1991). HH46 IRS shows a particularly broad profile, resembling the massive protostar W33A. Like W33A, HH46 IRS shows an absorption feature at $4.62 \mu\text{m}$, likely attributed to the OCN^- species. This molecule may be produced from HNC in the solid state at relatively low ice temperatures < 50 K (van Broekhuizen et al. 2004).

Concluding, while high temperature ice processing, traced by the CO_2 band, is not observed in the low mass envelopes, low temperature (< 50 K) processing may play a significant role. Qualitatively this is similar to some high mass protostars (W33 A, NGC7538 IRS9). The proposed evolutionary sequence of ice processing in massive envelopes (Boogert et al. 2000; van der Tak et al. 2000) is indeed largely based on high temperature indicators, such as ice crystallization, hot core gas temperatures and gas/solid state ratios. These relations need to

be investigated in a larger sample of low mass protostars, in which the CO_2 band profile is a crucial tracer.

4.2. $\text{CH}_3\text{OH}:\text{CO}_2$ Complexes

The long wavelength wing of the CO_2 bending mode may be a tracer of the presence of CH_3OH in the ices. CO_2 and CH_3OH form complexes, leading to an enhanced wing in some sources well fitted by laboratory ices with a $\text{CH}_3\text{OH}:\text{H}_2\text{O}:\text{CO}_2$ mixing ratio of 1:1:1 (e.g. W33A in Fig. 2b). Recently, large abundances of CH_3OH of 25% with respect to H_2O were found in the envelopes of some low mass protostars (Pontoppidan et al. 2003). Clearly, B5 IRS1 and HH46 IRS both have lower CH_3OH abundances (Table 1). This is consistent with the weakness of the long wavelength CO_2 wing. Indeed, laboratory mixtures with a $\text{CH}_3\text{OH}:\text{H}_2\text{O}:\text{CO}_2$ ratio of 0.3:1:1 fit the observed band well. The high $\text{CO}_2/\text{CH}_3\text{OH}$ column density ratio of ~ 6 toward these sources is however barely consistent with this laboratory mixture. Alternatively, the band profile can be explained by the combination of an abundant H_2O -rich ice responsible for the long wavelength wing, and an at least partly heated CO_2 -rich ice responsible for the crystallization substructures seen in HH46 IRS (Fig. 2c).

5. CONCLUSIONS AND FUTURE WORK

High quality SST observations of the CO_2 bending mode at $15 \mu\text{m}$ toward low mass protostars offer a new tracer of ice mantle composition and evolution. The embedded low mass systems B5 IRS1 and HH46 IRS show CH_3OH -poor ices with little evidence for 50-90 K thermal processing in their envelopes. Lower temperature processing appears evident in the solid CO band. These results form the basis for future studies on the physical and chemical state of ices entering protoplanetary disks, and how these and solar system ices are related. CO_2 bending mode observations of more evolved systems and edge-on disks are required.

Support for this work, part of the Spitzer Space Telescope Legacy Science Program, was provided by NASA through Contract Numbers 1224608 and 1230780 issued by the Jet Propulsion Laboratory, California Institute of Technology under NASA contract 1407. Astrochemistry in Leiden is supported by a NWO Spinoza grant and a NOVA grant.

REFERENCES

- Beichman, C. A., et al. 1984, *ApJ*, 278, L45
 Boogert, A. C. A., et al. 2000, *A&A*, 353, 349
 Boogert, A. C. A., Blake, G. A., & Öberg, K. 2004, *ApJ*, *in press*
 Brooke, T. Y., Sellgren, K., & Geballe, T. R. 1999, *ApJ*, 517, 883
 Charnley, S. B., Whittet, D. C. B., & Williams, D. A. 1990, *MNRAS*, 245, 161
 Chiar, J. E., et al. 2000, *ApJ*, 537, 749
 Ehrenfreund, P., Dartois, E., Demyk, K., & D’Hendecourt, L. 1998, *A&A*, 339, L17
 Evans, N. J., et al. 2003, *PASP*, 115, 965
 Gerakines, P. A., et al. 1999, *ApJ*, 522, 357
 Gibb, E. L., et al. 2000, *ApJ*, 536, 347
 Houck, J. R., et al. 2004, *ApJS*, this volume
 Hudgins, D. M., Sandford, S. A., Allamandola, L. J., & Tielens, A. G. G. M. 1993, *ApJS*, 86, 713
 Jørgensen, J. K., Schöier, F. L., & van Dishoeck, E. F. 2002, *A&A*, 389, 908
 Kessler, J. E., Hillenbrand, L. A., Blake, G. A., & Meyer, M. R. 2004, *ApJ*, *in press*
 Langer, W. D., Velusamy, T., & Xie, T. 1996, *ApJ*, 468, L41

- McLean, I.S., Becklin, E.E., Bendiksen, O., Brims, G., & Canfield, J. 1998, *Proc. SPIE*, 3354, 566
- Moorwood, A., et al. 1999, *The Messenger*, 95, 1
- Noriega-Crespo, A., et al. 2004, *ApJS*, this volume
- Ossenkopf, V. & Henning, T., 1994, *A&A*, 291, 943
- Pontoppidan, K. M., Dartois, E., van Dishoeck, E. F., Thi, W.-F., & d'Hendecourt, L. 2003, *A&A*, 404, L17
- Tielens, A. G. G. M., Tokunaga, A. T., Geballe, T. R., & Baas, F. 1991, *ApJ*, 381, 181
- van Broekhuizen, F. A., Keane, J. V., & Schutte, W. A. 2004, *A&A*, 415, 425
- van der Tak, F. F. S., van Dishoeck, E. F., Evans, N. J., & Blake, G. A. 2000, *ApJ*, 537, 283
- Werner, M. W., et al. 2004, *ApJS*, this volume
- Whittet, D. C. B., et al. 1996, *A&A*, 315, L357